



Trans. Nonferrous Met. Soc. China 34(2024) 3326-3343

Transactions of Nonferrous Metals Society of China

www.tnmsc.cn



Self-repairing Al₂O₃-TiO₂ coatings fabricated through plasma electrolytic oxidation with various cathodic pulse parameters

Mehri HASHEMZADEH^{1,2}, Keyvan RAEISSI¹, Fakhreddin ASHRAFIZADEH¹, Frank SIMCHEN², Amin HAKIMIZAD³, Monica SANTAMARIA⁴, Thomas LAMPKE²

- 1. Department of Materials Engineering, Isfahan University of Technology, Isfahan 84156-83111, Iran;
 - 2. Materials and Surface Engineering Group, Institute of Materials Science and Engineering, Chemnitz University of Technology, Chemnitz 09107, Germany;
- 3. Yekta Mobaddel Pars Co., Science and Technology Campus, Yazd University, Yazd 89158-18411, Iran;
- 4. Dipartimento di Ingegneria, Università di Palermo, Viale Delle Scienze, Ed. 6, 90128, Palermo, Italy

Received 5 March 2023; accepted 20 September 2023

Abstract: The influence of cathodic pulse parameters was evaluated on plasma electrolytic oxidation (PEO) coatings grown on 7075 aluminum alloy in a silicate-based electrolyte containing potassium titanyl oxalate (PTO) using pulsed bipolar waveforms with various cathodic duty cycles and cathodic current densities. The coatings were characterized by SEM, EDS, and XRD. EIS was applied to investigate the electrochemical properties. It was observed that the increase of cathodic duty cycle and cathodic current density from 20% and 6 A/dm2 to 40% and 12 A/dm2 enhances the growth rate of the inner layer from 0.22 to 0.75 μm/min. Adding PTO into the bath showed a fortifying effect on influence of the cathodic pulse and the mentioned change of cathodic pulse parameters, resulting in an increase of the inner layer growth rate from 0.25 to 1.10 µm/min. Based on EDS analysis, Si and Ti were incorporated dominantly in the upper parts of the coatings. XRD technique merely detected γ-Al₂O₃, and there were no detectable peaks related to Ti and Si compounds. However, the EIS results confirmed that the incorporation of Ti4+ into alumina changed the electronic properties of the coating. The coatings obtained from the bath containing PTO using the bipolar waveforms with a cathodic duty cycle of 40% and current density values higher than 6 A/dm² showed highly appropriate electrochemical behavior during 240 d of immersion due to an efficient repairing mechanism. Regarding the effects of studied parameters on the coating properties, the roles of cathodic pulse parameters and PTO in the PEO process were highlighted. Key words: Al₂O₃-TiO₂ coating; plasma electrolytic oxidation; potassium titanyl oxalate; electrochemical impedance spectroscopy

1 Introduction

The 7xxx series of Al alloys have an extensive application thanks to their high specific strength ratio. The 7075 aluminum alloy (AA7075) is one of the widely used high-strength alloys in the aerospace industry. Although the intermetallic particles of the alloy elements (Al, Mg, and Cu)

distributed in the Al matrix enhance its mechanical properties, they make the alloy be prone to different kinds of localized corrosion [1,2]. Anodization is a common technique for surface treatment of Al alloys to increase the thickness of oxide layer to be protective against corrosion attack. However, the electrochemical characterization of the intermetallic particles may vary during anodization owing to dealloying or anodic dissolution, which could make

Corresponding author: Mehri HASHEMZADEH, E-mail: mehri.hashemzadeh@mb.tu-chemnitz.de; Keyvan RAEISSI, E-mail: k raeissi@iut.ac.ir

the growth of a flawed alumina oxide [1].

Plasma electrolytic oxidation (PEO) is an advanced model of anodizing process and promotes durable, thick, uniform, more crystalline, and strongly adherent coatings on various types of metals especially the valve metals including Al, Mg, and Ti metals and their alloys [3]. There is significant progress in the industrialization of the PEO process owing to extensive studies that have been conducted in recent years [3]. The PEO process is commonly carried out in an environmentally friendly alkaline medium under high voltages, which trigger micro-discharges across the grown oxide [4,5]. It is well known that applying a pulsed bipolar current regime with an appropriate ratio of negative to positive charge quantities to Al and its alloys may lead to a soft-sparking mode and create fine, homogenous sparks promoting a thicker oxide layer [6].

The PEO method consists of a set of various processes with significantly different natures including chemical, electrochemical, and plasmachemical reactions, and also heat and mass transfer processes [7]. One of the most common drawbacks of the PEO coatings is their intrinsic porosity and micro-cracks allowing penetration of the corrosive solution toward the metal [8]. In addition, these flaws inside the alumina reduce the stiffness by an order of magnitude compared to fully dense alumina [9]. The literature review shows that the incorporation of titania into alumina improves its densification during thermal-involved processes including plasma spraying and PEO [10-14]. TiO₂ may incorporate into the PEO alumina coating by the addition of TiO₂ nanoparticles [15], or salt additives such as potassium titanyl oxalate [13,16], and dipotassium hexafluoro titanate [17] in the electrolytic solution. The stability of the electrolytic solution is highly important for the fabrication of reproducible coatings, which is significantly a necessary parameter for use on an industrial scale. Potassium titanyl oxalate (PTO) hydrolyzes in the alkaline solution and produces a colloidal solution, which is highly more stable than the suspension solution resulting from TiO₂ nanoparticles [13]. It has been observed that oxalates form a thicker double layer on the alumina/electrolyte interface [18,19]. This thick double layer shields the external electric field and then inhibits strong sparking induced by the strong external electric field and thereby, and finally develops a defect-free coating [20]. The fluoride-contained salt such as dipotassium hexafluoro titanate releases fluoride ions, which may promote the field-assisted ejection of Al³⁺ ions from the film surface and thereby reduces the efficiency of film growth [21]. Also, the HF gas evolution may occur during the PEO process due to the local acidification of the oxide/electrolyte interface. Considering these points, potassium titanyl oxalate can be a novel and environmentally safe additive for improving the quality of the PEO coatings.

Wear-resistant coatings are commonly fabricated in a dilute silicate solution using low-frequency (50 Hz) alternating current, which usually leads to a low growth rate and a relatively thick outer layer [22]. However, it has been stated that the bipolar pulses in the kHz range can provide sufficient control over plasma chemical processes occurring at the electrolyte/metal interface [15,22]. The short on-time pulse is more effective for the formation of intensively ionized plasma thanks to enhanced impact ionization [22].

In this work, the effect of cathodic pulse parameters including current density and duty cycle beside PTO impact was evaluated on the properties of the PEO coatings applied on AA7075 using high-frequency (2 kHz) bipolar waveforms in a silicate-based electrolytic solution. Based on the coating microstructure and literature review, a mechanism for the role of cathodic pulse and PTO additive in the PEO process was proposed.

2 Experimental

2.1 Sample preparation

The substrates were disk-shaped specimens of AA7075 with a diameter of 20 mm and thickness of 3 mm. Both flat sides of the specimens were ground mechanically using 1200-grit SiC paper. The substrates connected to a Cu wire were employed as the working electrode in the PEO process and washed in distilled water and degreased in ethanol before use.

2.2 PEO treatment

The PEO process was conducted using a switching power supply which had the ability to deliver adjustable unipolar and bipolar waveforms up to 750 V and 30 A for anodic pulse and -300 V

and -30 A for cathodic pulse. The experimental setup consisted of a 7 L stainless steel cylindrical cell which functioned as the counter electrode. The cell was positioned within a temperature-controlled container filled with 100 L of water. The electrolyte within the cell was continuously stirred using a submersible full polymer-body electrical pump. The electrolyte temperature was maintained at (20 ± 2) °C throughout the experiment. A solution containing 3 g/L sodium metasilicate pentahydrate $(Na_2SiO_3 \cdot 5H_2O, SMS)$ and 2 g/L KOH was used to produce reference coatings. In order to prepare the Al_2O_3 – TiO_2 composite, 3 g/L PTO $(K_2TiO_2O_4)_2 \cdot 2H_2O)$ was added to the reference electrolyte. Two samples with a total surface area of

 $0.19 \, \mathrm{dm^2}$ were simultaneously coated. The PEO treatments were conducted by applying four bipolar waveforms, which had the same anodic pulse parameters (average anodic current density of $6 \, \mathrm{A/dm^2}$ with a duty cycle of 20%) and different cathodic pulse parameters. A duty cycle is defined as the ratio between the on-duration in an anodic pulse or cathodic pulse during a single cycle to the total time of a cycle. Table 1 shows the cathodic pulse parameters including cathodic duty cycle (D_c) and average cathodic current density (J_c), and the waveforms recorded by oscilloscope. The specimen codes were defined based on the cathodic pulse parameters of the applied waveforms. The frequency of all waveforms was $2 \, \mathrm{kHz}$ and the

Table 1 Summary of specimen's codes, cathodic pulse parameters of applied waveforms, PTO concentration in PEO bath and recorded waveforms in PEO process

| Specimen code | $D_{\rm c}$ /% | $J_{\rm c}/({\rm A\cdot dm^{-2}})$ | $C_{\mathrm{PTO}}/(\mathrm{g}\!\cdot\!\mathrm{L}^{-1})$ | Recorded waveform |
|---------------|----------------|------------------------------------|---|--|
| I6D20 | 20 | 6 | 0 | 500 400 300 ≥ 200 mm mm mm = 15 10 5 0 ≤ |
| I6D20P | 20 | 6 | 3 | 100 0 100 -100 0 200 400 600 800 1000 Time/\(\mu\)s |
| I3D40 | 40 | 3 | 0 | 500 400 300 ≥ 200 |
| I3D40P | 40 | 3 | 3 | 100 -100 0 200 400 600 800 1000 Time/µs |
| I6D40 | 40 | 6 | 0 | 500 400 300 ≥ 200 15 10 5 0 ≤ |
| I6D40P | 40 | 6 | 3 | 100 -100 0 200 400 600 800 1000 Time/us |
| I12D40 | 40 | 12 | 0 | 500 400 300 \$ 200 |
| I12D40P | 40 | 12 | 3 | 100 -100 0 200 400 600 800 1000 Time/μs |

treatment time was 60 min. C_{PTO} in Table 1 states the PTO concentration in the PEO bath.

2.3 Coating characterization

The top-view surface and cross-sectional morphologies of the PEO coatings were observed using a field emission scanning electron microscope (FESEM FEI Quanta feIg 450; Hillsboro, USA) and scanning electron microscope (SEM LEO 1455VP; Zeiss, Jena, Germany), respectively. For the investigation of the cross-sections, the specimens were mounted in an epoxy resin vertically, ground through successive grades of SiC papers (up to 2400-grit), and then polished with a diamond past of 2.5 µm. After ultrasonically cleaning in ethanol, the specimens were dried in the cold-air flow. Energy dispersive spectroscopy (EDS) was used for the elemental analysis and mapping on crosssection of the coatings. The cross-section images were used for the measurement of the average thickness of the coatings by Image J 1.44p software.

X-ray diffraction (XRD) patterns were recorded using a X-ray diffractometer (Bruker, Billerica, USA) with a Co K_{α} radiation source (λ =0.179 nm, 40 kV, and 40 mA) in the Bragg–Brentano mode.

2.4 Evaluation of electrochemical behavior

The long-term electrochemical behavior of the coatings was evaluated by conducting electrochemical impedance spectroscopy (EIS) test using a potentiostat/galvanostat (AMETEK model PARSTAT 2273, Berwyn, USA). The corrosive solution was 3.5 wt.% NaCl with pH 4 adjusted by adding dilute HCl solution. The pH was established at 4 to increase corrosivity of the solution according to Ref. [23]. A standard three-electrode cell was set up that included a platinum plate and a saturated Ag/AgCl as the counter and reference electrodes, respectively. The prepared PEO coatings were the working electrode. The perturbation amplitude was 10 mV and the frequency range was from 10⁻² to 10⁵ Hz. The record of EIS responses was started after 24 h immersion in the mentioned corrosive solution and then was carried out at a regular interval of 7 d. Regarding that the EIS response was not changed significantly in a short-term period, the results related to the immersion time of 1, 30, 90, 150, and 240 d were reported. It is necessary to be mentioned that if one specimen fails before the 240th day, the EIS result of the failure day is presented. The corrosive solution was refreshed once a 7 d for maintaining its composition and pH constant.

3 Results and discussion

3.1 Voltage-time response

Figure 1 displays the effect of D_c , J_c , and PTO addition on the variation of amplitudes of anodic and cathodic voltages versus PEO processing time. At initial, the variation of anodic voltage is almost the same for all cases. The cathodic voltage is significantly lower than the anodic one. As known, aluminium oxide is an insulating material, which blocks the circulation of an anodic current if the electric field strength across the oxide is lower than the threshold required for the oxide growth under a high field. The latter in turn depends on the applied voltage and on the thickness. Under cathodic polarization, the metal is not going to be oxidized and thus the only option is the circulation of an electronic current. The electronic current can circulate across the oxide if the oxide Fermi level enters in the conduction band. Moreover, since the flat band potential of the Al₂O₃ is not exactly at the mid gap, but closer to the conduction band edge, the necessary current density to sustain a potential difference in absolute value is higher than that necessary under anodic polarization. When the electric field reaches the level of dielectric breakdown of the gas-steam shell surrounding the passive layer surface, micro-arc discharges initiate [24].

During the PEO process under D_c=40% (Figs. 1(b), (c) and (d)), a transient drop in anodic and cathodic voltage occurs. This sudden drop happens simultaneously with the appearance of soft sparking, which is detectable by the intensive decrease of micro-discharge intensity and acoustic emission. However, this behavior is transient and after about 1 min, the voltage starts to increase and the number and intensity of the sparks rise. The PEO process at 12 A/dm² and D_c =40% (I12D40 and I12D40P) shows a completely different voltagetime response after voltage drop and the behavior looks more similar to the soft-sparking (Fig. 1(d)). The gradual increase of the voltage is accompanied by the homogenous increase of spark intensity and acoustic emission. However, the transient voltage

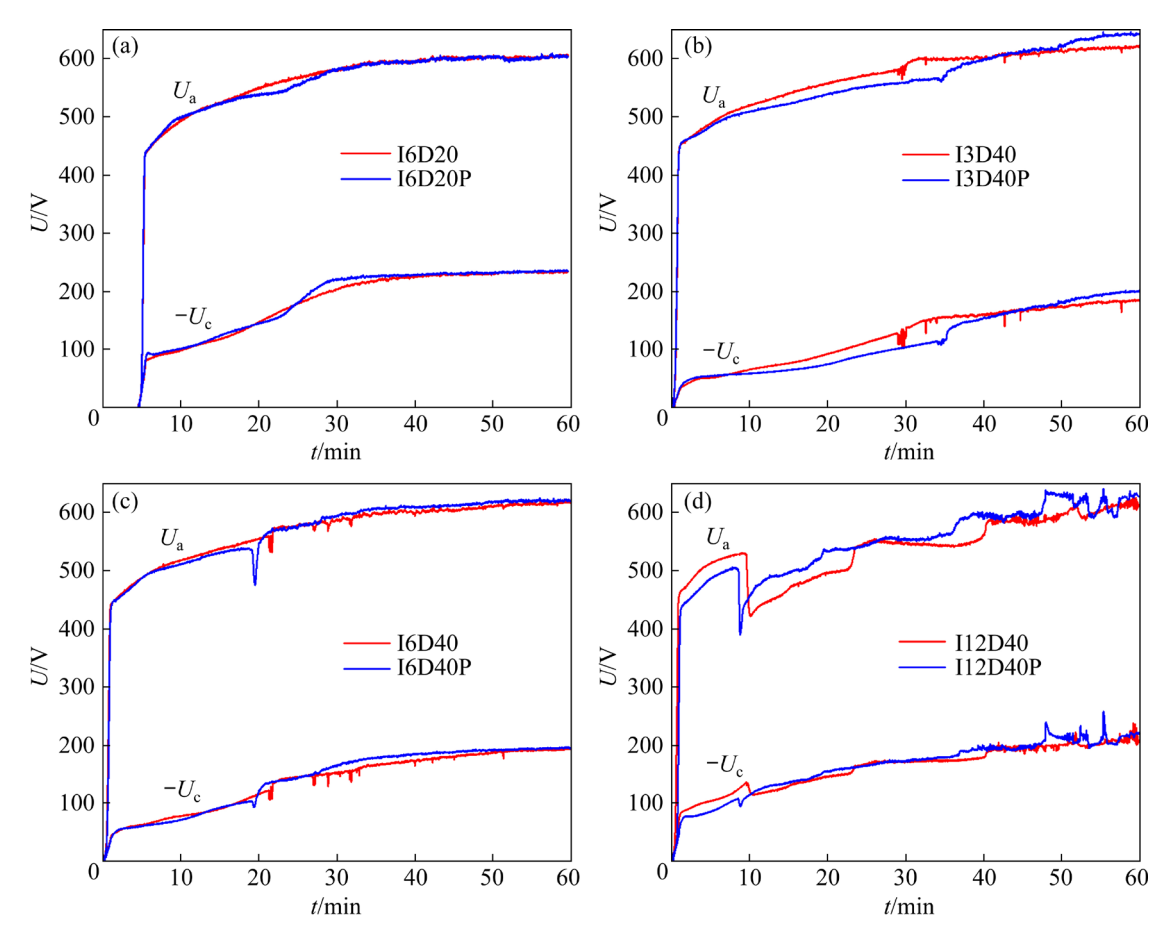


Fig. 1 Voltage—time (*U*–*t*) curves during PEO treatment of I6D20 and I6D20P (a), I3D40 and I3D40P (b), I6D40 and I6D40P (c), and I12D40 and I12D40P (d) specimens

drop and the sign of soft sparking are not seen at 6 A/dm^2 under D_c =20%, i.e. for I6D20 and I6D20P (Fig. 1(a)).

As seen in Fig. 1, the time and magnitude of the transient voltage drop depend on the cathodic current density and the presence of PTO in the bath. Regarding the voltage–time curves of PEO processes at 6, 12 A/dm² and D_c =40% (I6D40 and I12D40), presented in Figs. 1(c) and (d), it is interesting that doubling the J_c cuts in half the required time for voltage drop. Also, the presence of PTO in the bath decreases the required time for voltage drop except for I3D40P if compared with I3D40. It has been suggested that the soft-sparking occurs sooner when the growth rate is high [3]; therefore, it can be concluded that the increase of cathodic pulse and PTO encourages the transient soft-sparking because of promoting the growth rate.

3.2 Microstructure and phase constitution

Figure 2 displays the surface morphology of the as-prepared PEO coatings through the different waveforms and PTO addition. The surface exhibits the typical features of the PEO coatings obtained by a bipolar waveform, i.e. a combination of pancake structures rich in Al covered partially by nodules rich in electrolyte species and also volcano-like protrusions [25].

Furthermore, micro-cracks are observable on the coating surface as the result of thermal stress and high pressure during the PEO process [26]. However, according to Figs. 2(d) and (h), the surfaces of I12D40 and I12D40P specimens are covered by round-shaped precipitates, and no cracks are seen on the surface [27]. Pancake structure is created by strong micro-discharges occurring at the metal/coating interface and the central pore is most likely connected to the substrate [28,29]. The fine-distributed nodules are through interfacial micro-discharges occurring in pores and cracks on the surface [29]. Volcanoes are protuberances with asymmetrical shallow holes in their centre and are created only under a bipolar waveform and through discharges

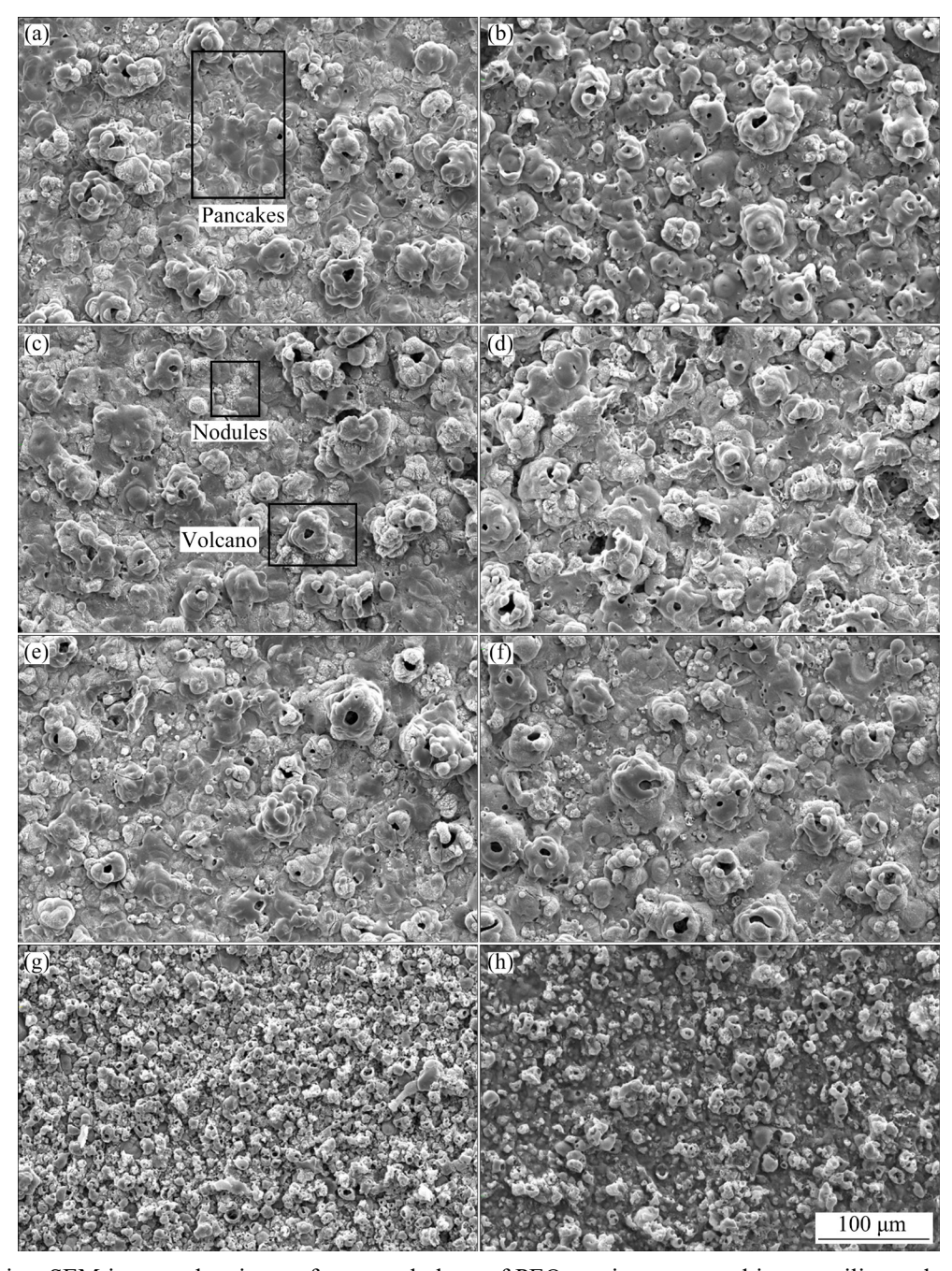


Fig. 2 Top-view SEM images showing surface morphology of PEO coatings prepared in pure silicate electrolyte (a-d) and silicate-PTO electrolyte (e-h) at cathodic duty cycle and cathodic current density of 20% and 6 A/dm² (a, e), 40% and 3 A/dm² (b, f), 40% and 6 A/dm² (c, g), 40% and 12 A/dm² (d, h), respectively

occurring at the upper parts of the inner layer [23,30,31].

As seen in Figs. 2(a) and (e), the coating surface at D_c =20% is largely dominated by the pancake structures surrounded by a few nodules. The increase of cathodic pulse parameters including duty cycle and current density or adding PTO reduces the number and size of the pancakes and develops more nodular and volcano features. It is noticeable that J_c =3 A/dm² promotes large pores on

the surface, especially in the presence of PTO.

Cross-sections SEM images of the PEO coatings are presented in Fig. 3. The bilayer structure of I6D20 and I3D40 specimens includes a fused outer layer and a compact inner layer with large pores between them (interfacial pores). As seen in Fig. 3(c), the I6D40 specimen shows an outer layer with a mixture of fused and sponge-like morphology along with a compact inner layer free of the interfacial pores. The fused morphology

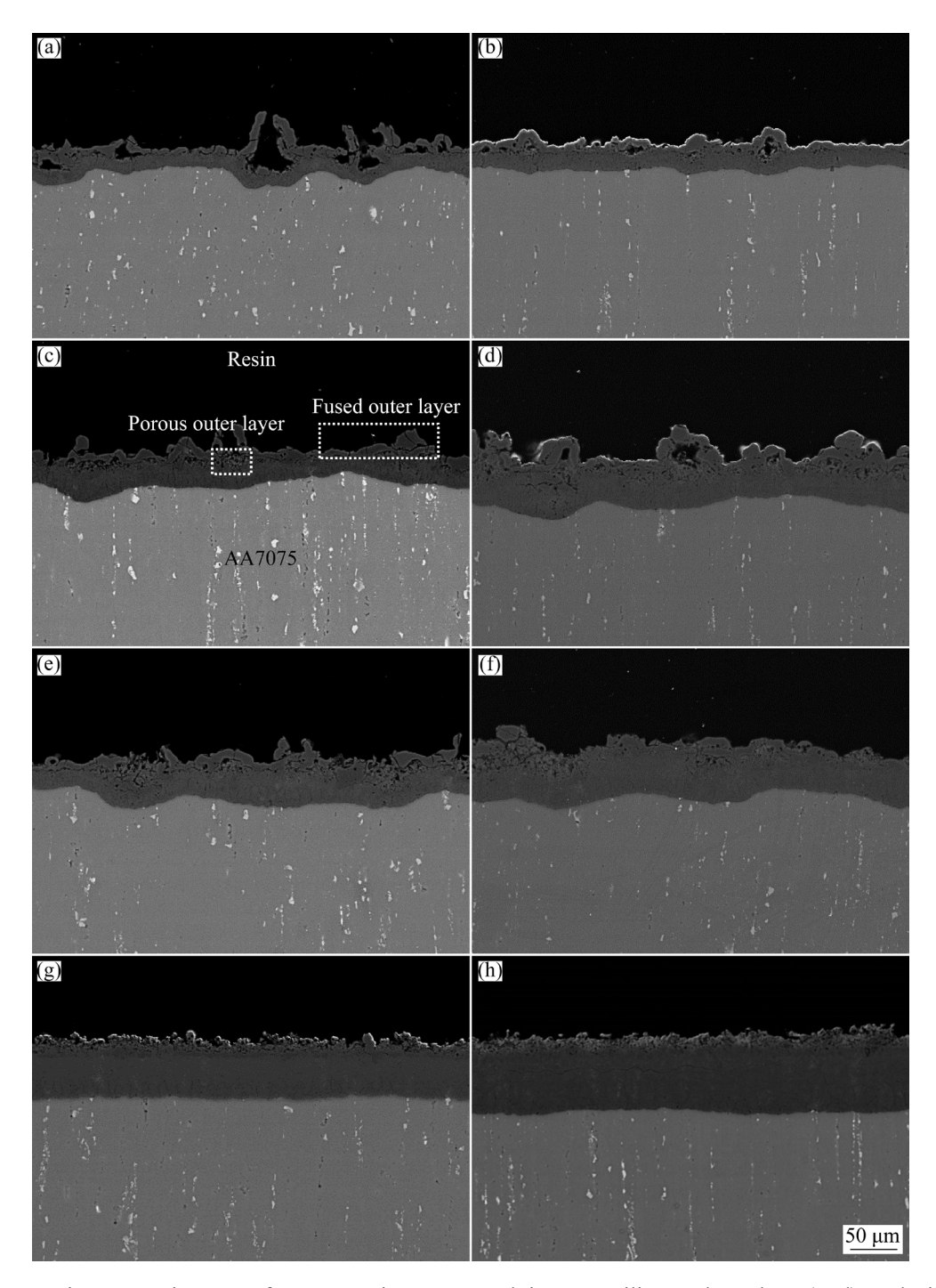


Fig. 3 Cross-section SEM images of PEO coatings prepared in pure silicate electrolyte (a–d) and silicate–PTO electrolyte (e–h) at cathodic duty cycle and cathodic current density of 20% and 6 A/dm² (a, e), 40% and 3 A/dm² (b, f), 40% and 6 A/dm² (c, g), and 40% and 12 A/dm² (d, h), respectively

completely disappears in the I12D40 specimen, while the sponge-like morphology develops (Fig. 3(d)). It has been suggested that the disappearance of the large interfacial pores occurs during the transient soft-sparking because Al-rich deposits fill them [32]. The increase of D_c and J_c parameters raises the inner layer thickness significantly.

Adding PTO into the bath does not considerably influence the thickness and the cross-sectional morphology of the coating prepared at J_c =6 A/dm² and D_c =20%. However, at D_c =40%, the fused characteristic of the outer layer transfers to be homogenous porous. The thickness values of the inner layer and outer layer of the coatings are displayed in a bar graph presented in Fig. 4. Overall,

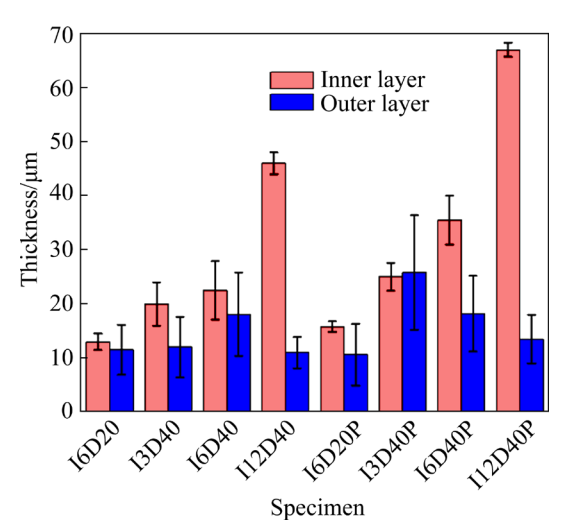


Fig. 4 Effect of cathodic pulse parameters and PTO addition on thickness of inner and outer layers of PEO coatings

the thickness of the inner layer is higher than the outer layer. The increase of cathodic pulse parameters is in favor of the inner layer growth so that the growth rate of the inner layer increases from 0.22 μ m/min for I6D20 to 0.75 μ m/min for I12D40. Adding PTO fortifies this effect and raises the growth rate of inner layer from 0.25 μ m/min for I6D20P to 1.10 μ m/min for I12D40P.

The mapping of elemental distribution out on the cross-section of the PEO coatings. Regarding Al

and O with a homogenous distribution on the crosssection of all coatings, only the distribution of Si and Ti is presented in Fig. 5.

As seen in Fig. 5, Ti and Si are incorporated dominantly in the outer part of the coatings. The incorporation of Si and Ti in the dense fused part of the outer layer is negligible in all coatings. Si is dominantly distributed at the bottom of the pores in the outer layer. Regarding the no-fused outer layer, there is a homogenous distribution of Si in the outer layer of the coatings grown at 12 A/dm² and D_c =40% (i.e. I12D40 and I12D40P). The Ti distribution shows a trend similar to that of the Si and dominantly incorporates the porous parts of the outer layer. It is obvious that the increase of cathodic pulse parameters and PTO addition inhibit the growth of the dense fused morphology; thereby they lead to an even distribution of the electrolyte species in the outer layer.

As stated in the literature [29,33], silicate forms silica gel on the alumina surface and incorporates into the growing oxide through interfacial discharges occurring inside the cracks and pores. Simultaneously, the PTO hydrolyzes and produces a colloidal solution containing greatly fine TiO₂ nano-particles and oxalate anions [13]. In our previous research [13], it was observed that Ti is distributed homogenously in a cross-section of the

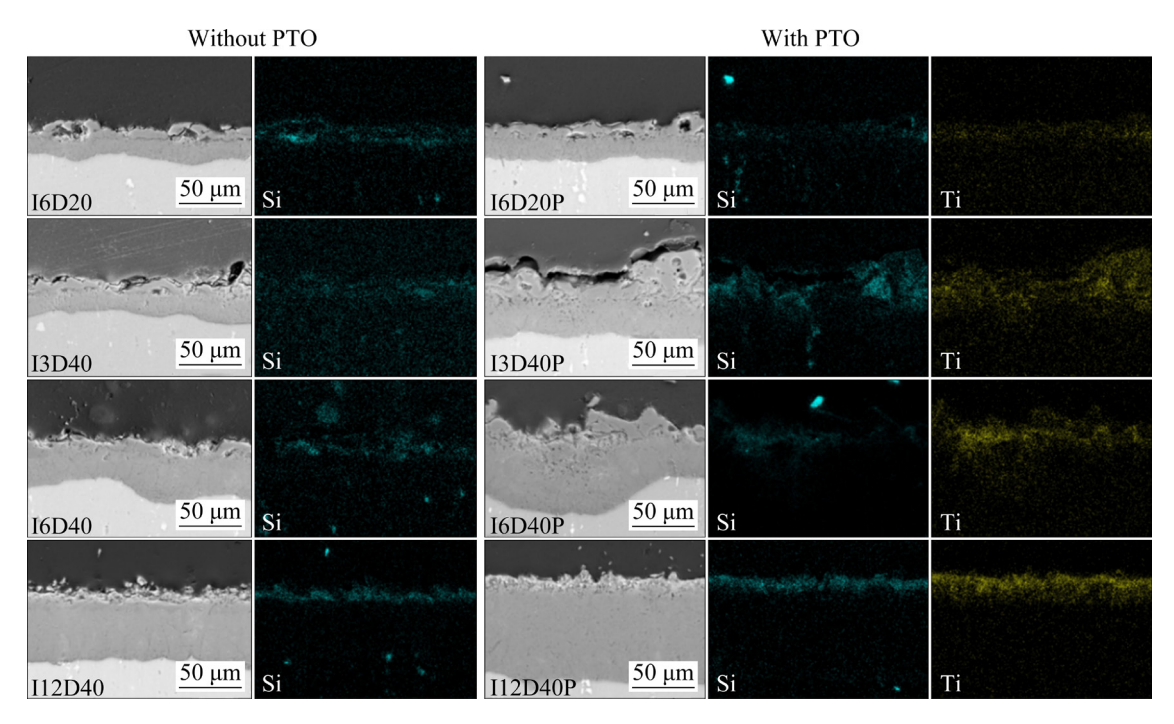


Fig. 5 Si and Ti distribution in PEO coatings prepared in bath without PTO and with 3 g/L PTO at different cathodic pulse parameters

coating prepared by unipolar waveform, which is attributed to its capability for the incorporation through all kinds of micro-discharges. As TiO₂ has a negative zeta potential in an alkaline medium, the cathodic pulse imposes a repelling force on TiO₂ particles; therefore, their incorporation under the bipolar waveforms is significantly lower than the unipolar one and is dominantly on the porous parts of the outer layer.

The phase composition of the coatings was determined using the XRD technique. Because the XRD patterns are similar, only those for I12D40 and I12D40P specimens are reported as seen in Fig. 6 (the rest are presented in Fig. S1 of the Supplement Materials (SM)).

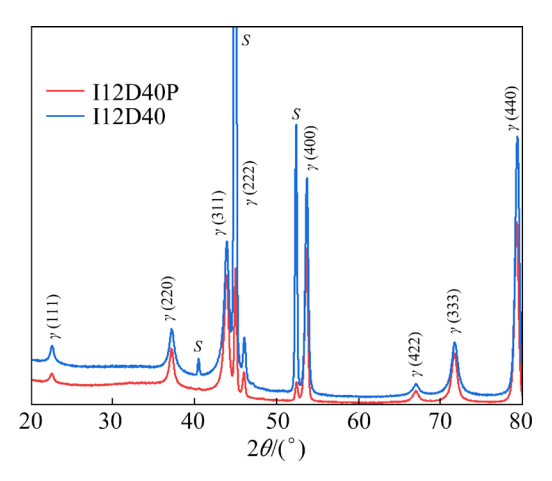


Fig. 6 XRD patterns of I12D40 and I12D40P specimens (*S* shows peaks related to substrate)

In all specimens, the peaks related to the substrate and γ -Al₂O₃ responded by the coating body are detected. The changes of D_c and J_c do not change the XRD patterns and only influence the intensity of substrate peaks due to the variation of coating thickness. There are no peaks related to the Si component because the higher glass-forming ability of Si leads to Si incorporation as an amorphous phase [34]. Adding PTO makes the intensity of γ -Al₂O₃ (γ phase) peaks extremely weaker; meanwhile, no peak belonging to Ti components appears due to doping into alumina and forming a polymeric titanium oxide on the coating surface [13,20].

3.3 Long-term EIS data

Bode phase and Bode |Z| (Z is the magnitude of complex impedance) plots of the alumina and

alumina-titania coatings at different immersion time up to 240 d in 3.5 wt.% NaCl solution (adjusted at pH 4) are presented in Figs. 7 and 8, respectively. After 1 d of immersion, the coatings reveal one semi-asymmetric broad hump in the middle-frequency region of 10 kHz-0.1 Hz, attributed to the overlap of two capacitive responses from their inner and outer layers. However, I6D20P coating shows two separate humps (Fig. 8(a)). In addition, there is an increase in phase angle above 10 kHz for all coatings, which might be owing to an experimental artifact originated by the parasitic capacitance of the measurement cables and the cell [35]; therefore, it would not be discussed. In Bode |Z| plots of all coatings, there is a transmission behavior from capacitive to resistive at low frequencies, indicating the local ingress of the aggressive solution toward the substrate through the micro-pores.

For I6D20 coating, by increasing immersion time, the broad hump responded by the outer and inner layers separates into two distinguished humps (Fig. 7(a)), while for others, it shifts to the lower frequencies and also more negative phase angles (about -75°). It should be noticed that this shift is also observed for the two humps of I6D20P coating (Fig. 8(a)). These changes in Bode phase plots are also associated with the disappearance of resistive behavior in the low-frequency region on Bode |Z| plots. These are indications of an improvement in corrosion barrier performance. This denotes that a repairing mechanism is governed by longer immersion time. After 150 d of immersion, the I6D20 coating exhibits two different humps located in 10 Hz-1 kHz and 0.3-0.01 Hz ranges at phase angles of about -65° and -30°, respectively, where the low-frequency hump is resulted by the local corrosion attack on the aluminum substrate [36]. Thus, the I6D20 specimen is exposed to pitting corrosion after 150 d. The pitting also occurs for the I6D20P coating after 190 d (Figs. 8(a) and (a')). However, the I3D40, I6D40, and I12D40 coatings lose their protection after 240 d of immersion, while I6D40P and I12D40P show no decay in protective action during the 240 d immersion. At 30 and 90 d of immersion, the Bode phase plot of I12D40P coating (Figs. 8(d)) shows a flat part in the lowfrequency region beside the hump in middle to low frequencies. This flat part is due to the formation of

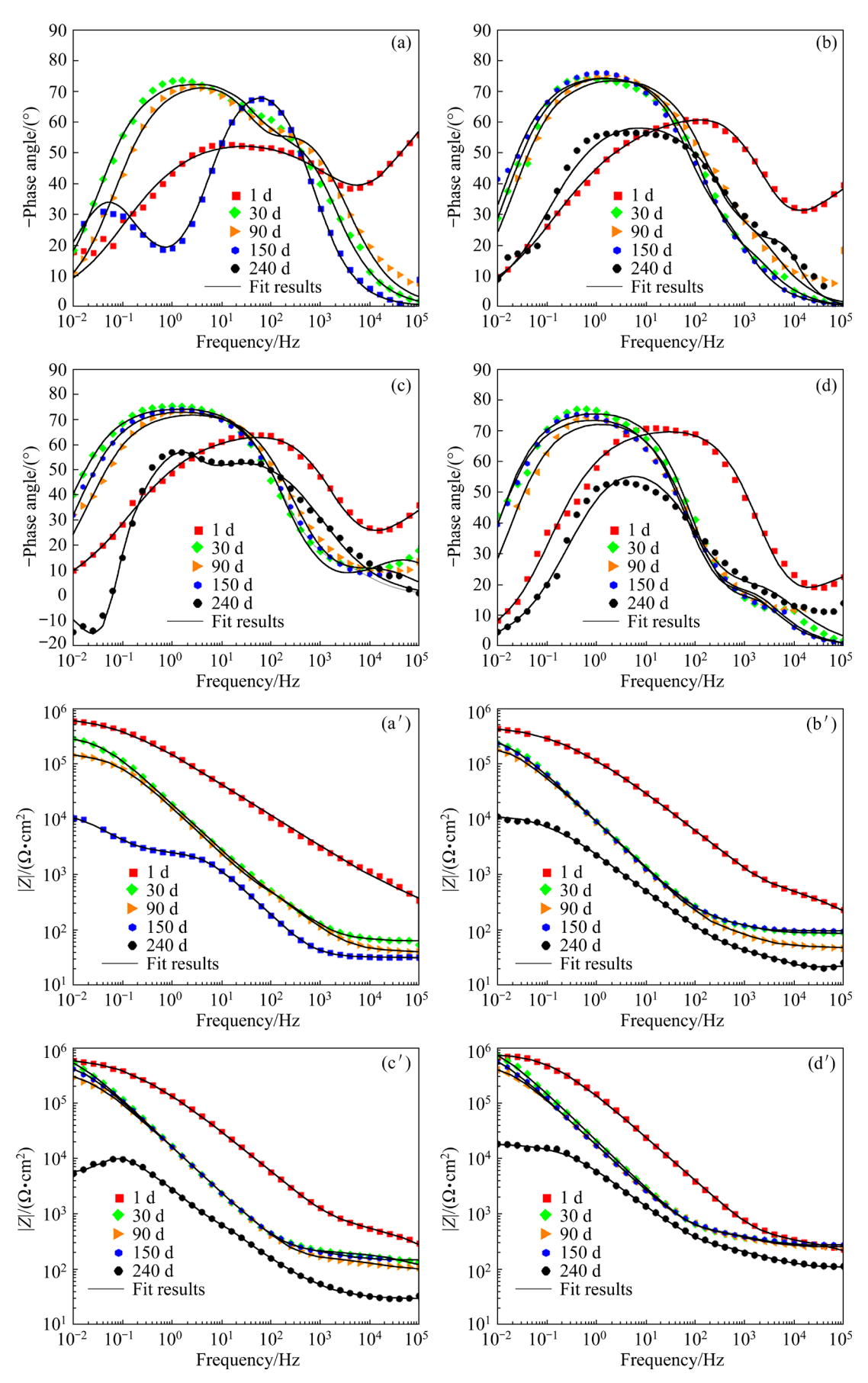


Fig. 7 Bode phase (a-d) and |Z| (a'-d') plots of as-prepared alumina coatings including I6D20 (a, a'), I3D40 (b, b'), I6D40 (c, c'), and I12D40 (d, d') immersed in 3.5 wt.% NaCl solution at pH 4 for different time

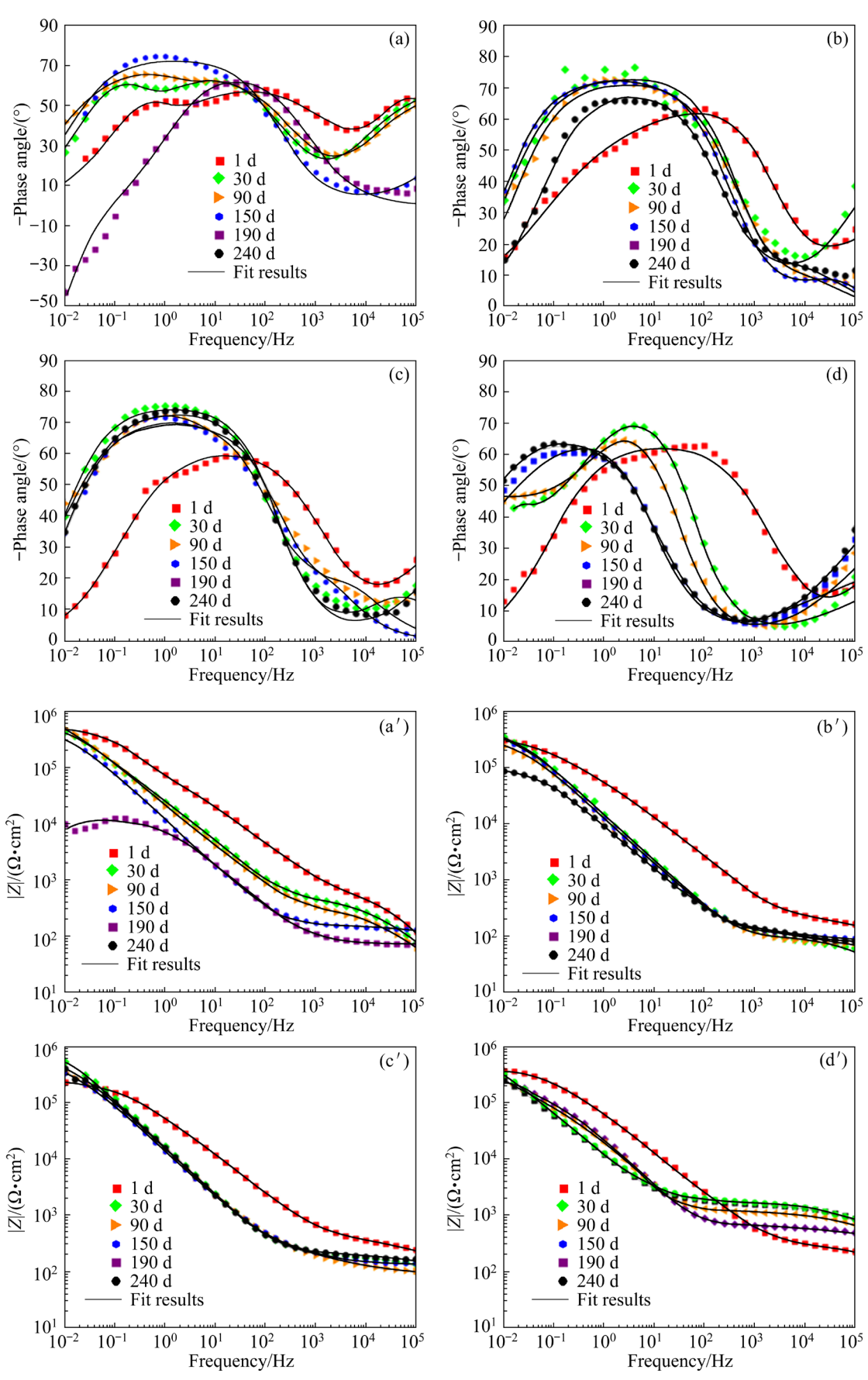


Fig. 8 Bode phase (a–d) and |Z| (a'–d') plots of as-prepared alumina–titania coatings including I6D20P (a, a'), I3D40P (b, b'), I6D40P (c, c'), and I12D40P (d, d') immersed in 3.5 wt.% NaCl solution at pH 4 for different time

a diffusion layer [36]. This diffusion response disappears after 150 d and a hump appears in the middle to low frequency region, as seen in Fig. 8(d).

The EIS results are simulated using equivalent electrical circuits (ECs) shown in Fig. 9 and the extracted data are presented in Tables S1–S8 in SM. Regarding the overlap of the capacitive loops on the first day of immersion, an EC with one time constant (Fig. 9(a)) is used for fitting the EIS responses except for I6D20P. The ECs related to the failure of the coatings are reported in Fig. S2 in SM.

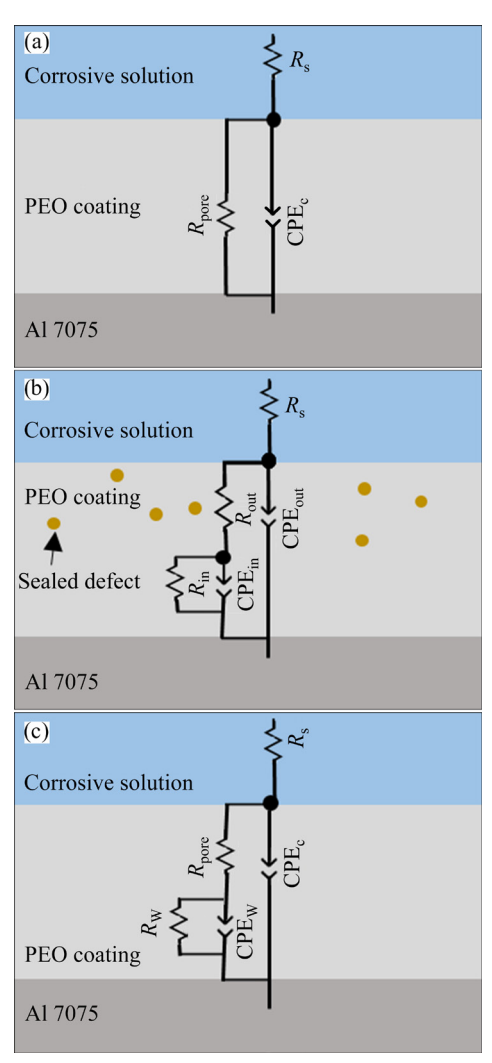


Fig. 9 ECs used for simulation of EIS data of Figs. 7 and 8: (a) EC for simulation of porous PEO layer; (b) EC for simulation of PEO layer with sealed defects; (c) EC for simulation of diffusion of corrosive solution through PEO inner layer

In Fig. 9, R_s , R_{pore} , R_{out} , and R_{in} are the uncompensated solution resistance, pore resistance, outer layer resistance, and inner layer resistance, respectively. CPE_c, CPE_{out}, and CPE_{in} are related to

the constant phase elements of the defective coating, outer layer, and inner layer, respectively. Also, W is the Warburg element denoting the semi-infinite length of diffusion, and $R_{\rm W}$ and CPE_W are the Warburg impedance and the constant phase element associated with diffusion processes, respectively.

The variation of polarization resistance (sum of the resistances) of the coatings and the C_x value (C_x is the capacitance of the PEO coating) of their inner layer during the immersion are displayed in Fig. 10. The capacitance and polarization resistance (R_p) values are indicators of the protective performance and reflect the barrier properties of the coatings. The high resistance and low capacitance reveal that the coating is more protective [37].

It is noticeable that despite the higher thickness, each coating prepared in the presence of PTO shows lower polarization resistance (R_p) and higher capacitance compared to their reference coating during the first day of immersion. This might be due to the change of electronic properties of the alumina via doping by Ti⁴⁺. The substitution of Ti⁴⁺ with Al³⁺ leads to the formation of donor and acceptor levels at the impurity points and compensating cation vacancies, respectively. These levels readily support charges for conduction or polarization; in this way, ionization of the donors releases electrons while positive holes capture electrons from the valance band. This charge transfer leads to interfacial polarization which increases the dielectric constant [38]. mechanism can be assumed if it is considered that a low amount of impurities, about 0.5 wt.%, is more than enough to produce substantial electrical charges [38]. Moreover, after 1 d of immersion, the polarization resistance of the coatings prepared by bipolar waveforms is extremely lower $(R_p \le 1 \text{ M}\Omega \cdot \text{cm}^2)$ than that of the coating grown using unipolar waveform ($\sim 10 \,\mathrm{M}\Omega \cdot \mathrm{cm}^2$) at the same anodic pulse reported in our previous work [13]. This is so strange if considering that the bipolar coatings are thicker and more compact than the unipolar coating. It is well established that the thin barrier layer attached to the substrate provides most of the total corrosion performance in the PEO coatings [39]. Therefore, it seems that the damage occurs in the barrier layer through the cathodic pulse. However, the repairing mechanism during the immersion occurs in the bipolar coatings, which considerably improves the electrochemical behavior.

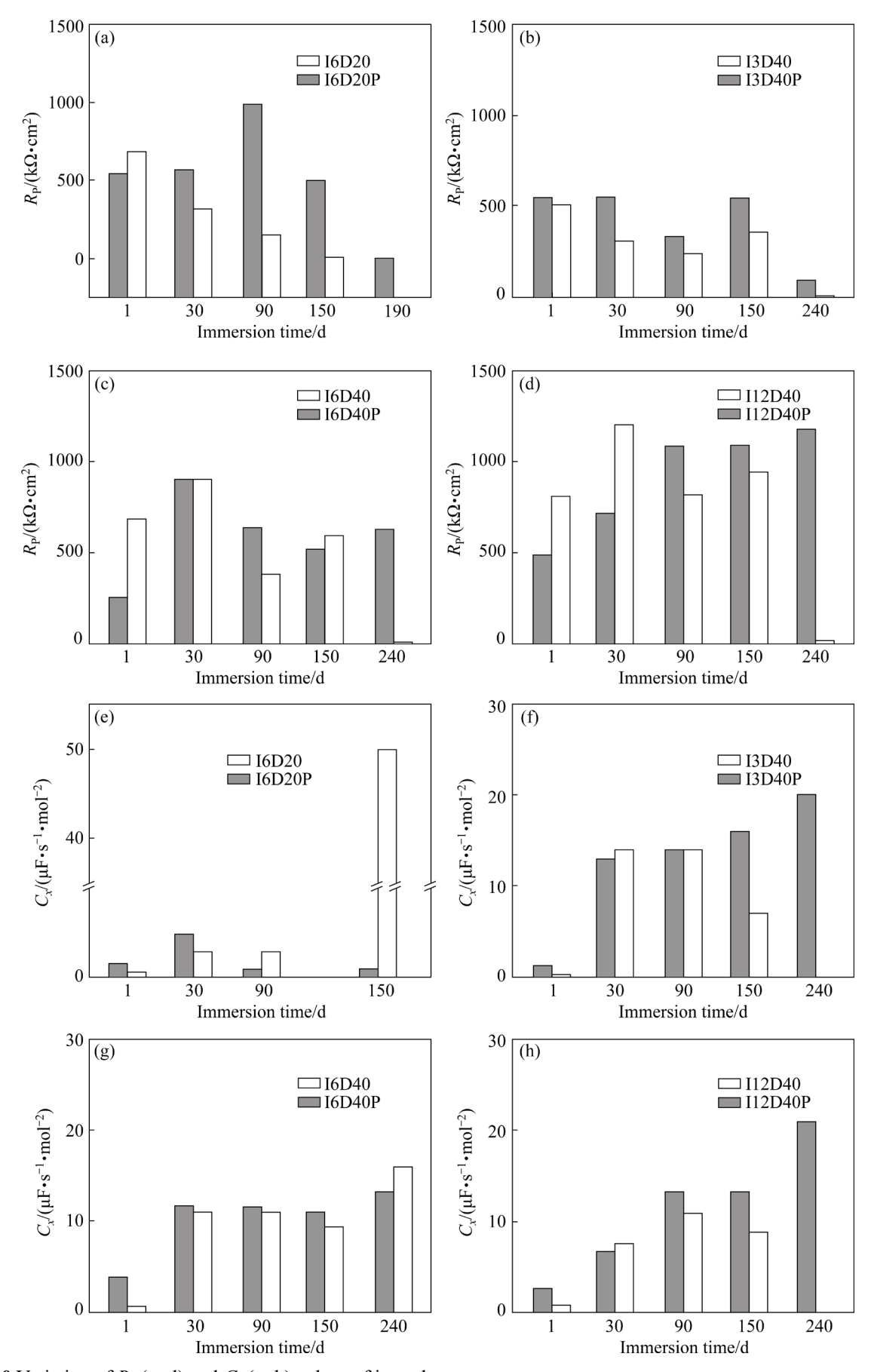


Fig. 10 Variation of R_p (a-d) and C_x (e-h) values of inner layer

In this way, voluminous hydrated alumina might be formed by the reaction between the anhydrous alumina and the adsorbed water [40]. These self-sealing products raise polarization resistance through the blocking of the paths available for penetration of the aggressive solution toward the substrate. As seen, the I6D40P and I12D40P coatings show a polarization resistance higher than $500 \text{ k}\Omega \cdot \text{cm}^2$ during the prolonged immersion time, because, they show stable and better self-sealing during immersion time. This approves that these coatings have relatively small imperfections that can readily be blocked [15]. The appropriate microstructure of these two coatings is attributed to the even sparking promoted by oxalate and the sintering facilitation of alumina by the doped Ti⁴⁺.

3.4 Role of cathodic pulse and PTO in PEO process

Despite the significant research conducted on the role of the cathodic pulse, the accurate role of the cathodic pulse in the PEO process is not so clear [3]. However, it is well-known that the cathodic pulse leads to a higher growth rate and lower porosity in alumina PEO coatings [6]. One proposed reason is that the cathodic pulse impedes excessive charge accumulation on the coating surface, which results in large discharges [41]. A fascinating phenomenon during PEO of aluminum alloys under bipolar waveform with an optimum electrolyte and electrical parameters is the softsparking mode, which is accompanied by a decrease of anodic voltage and acoustic emission [6]. Soft-sparking leads to a more uniform discharge distribution over the sample surface and therefore develops a hard, thick, and dense coating [6,41,42].

In spite of equal cathodic electrical charge in the I6D20 and I6D40 processes, the voltage—time curve and the characteristics of the coatings are completely different. Regarding the lower growth rate of I6D20 and I6D20P than that of I6D40, it can be suggested that the cathodic current dominantly results in hydrogen evolution at the coating/electrolyte interface. However, for I6D40, H⁺ could diffuse into the coating and change the coating properties. This is suggested regarding the proton conductivity of alumina coating [42].

As observed in Fig. 3, the increase of cathodic pulse parameters (including D_c and J_c), and also PTO addition increase the growth rate of the inner

layer. Since the coatings prepared in the absence and presence of PTO under the same waveform show almost the same surface morphology, it can be concluded that a part of PTO's role in the PEO process is similar to that of the cathodic pulse. In the initial time of the PEO process, the coating has sufficiently high electronic conductivity to support hydrogen evolution during the cathodic pulse. When the coating thickens enough, it may be considered resistant to arriving electrons from the metal/coating interface to the coating/electrolyte interface [42]. ROGOV et al [42] proposed that local acidification of the electrode surface due to the low rate of hydrogen evolution rearranges the electrical double layer at the oxide/electrolyte interface, which leads to a decrease and an increase of the potential barrier in anodic and cathodic directions, respectively. As seen in Fig. 1, instead of an increase, the drop in cathodic voltage occurs in coincidence with the drop of anodic voltage, which indicative of the increase in electrical conductivity in both directions. Then, it can be concluded that the rearrangement of the electrical double layer is not the reason for the voltage drop in this study. This might be due to the high frequency of the waveforms (2 kHz), which makes the rearrangement of the electrical double layer impossible. This is in agreement with the observation of NOMINÉ et al [41]. Regarding the literature and the observations in this project, a mechanism is proposed for the role of cathodic pulse and PTO additive during the PEO process as follows: As stated before, in valve metals, the electrons can flow through the oxide layer when the metal is the cathode. This process is limited by the increase in coating thickness and the decrease in electronic conductivity. Therefore, after the coating thickens enough, the electrons flow in the oxide during the cathodic pulse and acidification occurs at the oxide/electrolyte interface. Alumina-silicate surface is prone to be dissolved in an acidic medium and then a porous outer layer forms [43]. The porous outer layer could facilitate the diffusion of H⁺ ions into the oxide. The increase of cathodic current increases the growth rate and facilitates the formation of a thicker layer. The higher acidification induced by water dissociation makes more porosities and thus higher diffusion of H⁺ ions into the oxide. These ions could combine with the electrons at the metal/coating interface and release H₂. The H₂ evolution could destroy the barrier layer continuity at the metal/oxide interface; therefore, the increase in mass and charge transfer rates leads to an increase in growth rate at this interface.

At 6 A/dm^2 and $D_c=20\%$, the short time of cathodic pulse (100 µs) might not be sufficient for local acidification of the electrode surface and then a fused dense outer layer is developed. This mechanism is in agreement with the results of the research conducted by GEBAROWSKI and PIETRZYK [44]. They observed a significant change in the electrical properties of the oxide coating prepared under the soft sparking transition. Before soft sparking, the coating significantly showed high resistance (order of $M\Omega$) for charge and mass transfer. However, the experiencing soft sparking had extremely less resistance and higher capacitance. The authors attributed this to the formation of some defects in the barrier layer that destroys the barrier layer continuity due to the hydrogen evolution during the cathodic pulse. In addition, the smooth metal/coating interface seen in Figs. 3(d) and (h) shows the lack of diffusion barrier at the metal/coating interface of the coatings grown at 12 A/dm^2 and $D_c=40\%$ (i.e. I12D40 and I12D40P) due to the highly defective barrier layer.

As seen in Fig. 3, PTO enhances the cathodic pulse effect. It is noticeable that the role of PTO is prominent at higher D_c and J_c . It has been confirmed that organic acids and their conjugate salts could make a considerable influence on various types of minerals and enhance elemental mobility and intensify the solid matrix solubility. For instance, the adsorption of oxalate as a bidentate chelator on alumina weakens the Al-O bonds by polarizing bridging Al—O bonds, which is called oxalate-promoted dissolution of the oxide minerals [45]. In addition, it was shown that the proton-promoted dissolution rate in the presence of oxalate could be significantly high [43]. Thus, it can be concluded that the proton-promoted alumina dissolution induced by cathodic pulse, oxalatepromoted alumina dissolution, and synergistic effect of oxalate on the proton-promoted alumina dissolution make the fused dense layer as a barrier for H⁺ penetration into the growing oxide and develop the porous layer. In this way, the H₂ evolution at the metal/oxide interface intensifies the defective barrier layer and helps the coating growth.

Also, regarding that the dense fused layer is more likely leading to the spallation of the coating during the PEO process [20,31,46], it can be suggested that the porous outer layer is useful for the even distribution of the sparks created during the anodic pulse and also the porous layer is more capable for accommodating the volume expansion of the oxide formation.

As stated, the soft sparking transient did not occur in the PEO processes at 6 A/dm^2 and D_c =20% (i.e. I6D20 and I6D20P), which might be due to the lack of required acidification during the short cathodic pulse. The higher compactness of I6D20 and I6D20P coatings in comparison with that of the coatings prepared by the unipolar waveform at the same anodic pulse [13], is owing to the modification of anodic sparks by cathodic pulse through prevention of excessive charge accumulation on the coating.

4 Conclusions

(1) A higher growth rate of PEO coating was achieved by designing an appropriate cathodic pulse of bipolar waveform and adding potassium titanyl oxalate into the PEO electrolyte. The cathodic duty cycle and cathodic current density influence the growth rate of the inner layer significantly. This was accompanied by the changing of the surface morphology of the coating from a fused-dense morphology to a homogenous porous morphology.

(2) By XRD analysis, only γ -Al₂O₃ was found in the coatings and no crystalline Ti-containing was detected. EIS results revealed that the PTO addition into the bath made Ti⁴⁺ incorporation as point defects into alumina crystal lattice, which led to a lower polarization resistance and higher CPE values after 1 d of immersion in the corrosive solution. The cathodic duty cycle of 40% and cathodic current density values more than 6 A/dm² along with adding PTO in the PEO bath developed coatings that showed a repairing mechanism during immersion and protected the substrate from the corrosive solution during immersion of 240 d.

CRediT authorship contribution statement

Mehri HASHEMZADEH: Formal analysis, Investigation, Methodology, Software, Validation, Writing – Original draft; **Keyvan RAEISSI:** Data

curation, Project administration, Supervision, Validation, Visualization, Writing – Review & editing; Fakhreddin ASHRAFIZADEH: Data curation, Supervision, Validation, Visualization, Writing – Review & editing; Frank SIMCHEN: Validation, Writing – Review & editing; Amin HAKIMIZAD: Validation, Writing – Review & editing; Monica SANTAMARIA: Conceptualization, Validation, Visualization, Writing – Review & editing; Thomas LAMPKE: Supervision, Validation, Writing – Review & editing.

Declaration of competing interest

The authors declare that they have no known competing financial interests or personal relationships that could have appeared to influence the work reported in this paper.

Supplementary Materials

Supplementary Materials in this paper can be found at: http://tnmsc.csu.edu.cn/download/16-p3326-2023-0264-Supplementary Materials.pdf.

References

- [1] ZHANG F, ÖRNEK C, NILSSON J O, PAN J S. Anodisation of aluminium alloy AA7075: Influence of intermetallic particles on anodic oxide growth [J]. Corrosion Science, 2020, 164: 108319.
- [2] JUNGE T, LIBORIUS H, MEHNER T, NESTLER A, SCHUBERT A, LAMPKE T. Measurement system based on the Seebeck effect for the determination of temperature and tool wear during turning of aluminum alloys [J]. Procedia CIRP, 2020, 93: 1435–1441.
- [3] CLYNE T W, TROUGHTON S C. A review of recent work on discharge characteristics during plasma electrolytic oxidation of various metals [J]. International Materials Reviews, 2019, 64: 127–162.
- [4] SIEBER M, SIMCHEN F, MORGENSTERN R, SCHARF I, LAMPKE T. Plasma electrolytic oxidation of high-strength aluminium alloys: Substrate effect on wear and corrosion performance [J]. Metals, 2018, 8: 356.
- [5] YEROKHIN A L, VOEVODIN A A, LYUBIMOV V V, ZABINSKI J, DONLEY M. Plasma electrolytic fabrication of oxide ceramic surface layers for tribotechnical purposes on aluminium alloys [J]. Surface and Coatings Technology, 1998, 110: 140–146.
- [6] JASPARD-MÉCUSON F, CZERWIEC T, HENRION G, BELMONTE T, DUJARDIN L, VIOLA A, BEAUVIR J. Tailored aluminium oxide layers by bipolar current adjustment in the plasma electrolytic oxidation (PEO) process [J]. Surface and Coatings Technology, 2007, 201: 8677–8682.
- [7] MATYKINA E, ARRABAL R, SCURR D J, BARON A, SKELDON P, THOMPSON G E. Investigation of the mechanism of plasma electrolytic oxidation of aluminium

- using ¹⁸O tracer [J]. Corrosion Science, 2010, 52: 1070–1076.
- [8] AKBARZADEH S, SOPCHENSKI SANTOS L, VITRY V, PAINT Y, OLIVIER M G. Improvement of the corrosion performance of AA2024 alloy by a duplex PEO/clay modified sol-gel nanocomposite coating [J]. Surface and Coatings Technology, 2022, 434: 128168.
- [9] CURRAN J A, CLYNE T W. Porosity in plasma electrolytic oxide coatings [J]. Acta Materialia, 2006, 54: 1985–1993.
- [10] MICHALAK M, ŁATKA L, SOKOŁOWSKI P, CANDIDATO R T, AMBROZIAK A. Effect of TiO₂ on the microstructure and phase composition of Al₂O₃ and Al₂O₃-TiO₂ APS sprayed coatings [J]. Bulletin of the Polish Academy of Sciences, 2021, 69: 136735.
- [11] TING C H, CHOU Y T, RAMESH S, SOPYAN I, TENG W D. Sintering behaviour of TiO₂-doped alumina for biomedical application [C]//Proceedings of the 4th Kuala Lumpur International Conference on Biomedical Engineering. Heidelberg: Springer, 2008: 351–353.
- [12] BIAN Han-min, YANG Yong, WANG You, TIAN Wei. Preparation of nanostructured alumina–titania composite powders by spray drying, heat treatment and plasma treatment [J]. Powder Technology, 2012, 219: 257–263.
- [13] HASHEMZADEH M, RAEISSI K, ASHRAFIZADEH F, HAKIMIZAD A, SANTAMARIA M. Incorporation mechanism of colloidal TiO₂ nanoparticles and their effect on properties of coatings grown on 7075 Al alloy from silicate-based solution using plasma electrolytic oxidation [J]. Transactions of Nonferrous Metals Society of China, 2021, 31: 3659–3676.
- [14] BAHRAMIAN A, RAEISSI K, HAKIMIZAD A. An investigation of the characteristics of Al₂O₃/TiO₂ PEO nanocomposite coating [J]. Applied Surface Science, 2015, 351: 13–26.
- [15] HAKIMIZAD A, RAEISSI K, ALI GOLOZAR M, LU X P, BLAWERT C, ZHELUDKEVICH M L. The effect of pulse waveforms on surface morphology, composition and corrosion behavior of Al₂O₃ and Al₂O₃/TiO₂ nano-composite PEO coatings on 7075 aluminum alloy [J]. Surface and Coatings Technology, 2017, 324: 208–221.
- [16] AKBARI E, DI FRANCO F, CERAOLO P, RAEISSI K, SANTAMARIA M, HAKIMIZAD A. Electrochemicallyinduced TiO₂ incorporation for enhancing corrosion and tribocorrosion resistance of PEO coating on 7075 Al alloy [J]. Corrosion Science, 2018, 143: 314–328.
- [17] TANG Ming-qi, LI Wei-ping, LIU Hui-cong, ZHU Li-qun. Influence of K₂TiF₆ in electrolyte on characteristics of the microarc oxidation coating on aluminum alloy [J]. Current Applied Physics, 2012, 12: 1259–1265.
- [18] KASEEM M, KWON J H, KO Y G. Modification of a porous oxide layer formed on an Al–Zn–Mg alloy via plasma electrolytic oxidation and post treatment using oxalate ions [J]. RSC Advances, 2016, 6: 107109–107113.
- [19] HUSSAIN T, KASEEM M, KO Y G. Hard acid-hard base interactions responsible for densification of alumina layer for superior electrochemical performance [J]. Corrosion Science, 2020, 17: 108663.
- [20] HASHEMZADEH M, RAEISSI K, ASHRAFIZADEH F, SIMCHEN F, HAKIMIZAD A, SANTAMARIA M,

- LAMPKE T. The importance of type of Ti-based additives on the PEO process and properties of Al₂O₃–TiO₂ coating [J]. Surfaces and Interfaces, 2023, 36: 102523.
- [21] ELAISH R, CURIONI M, GOWERS K, KASUGA A, HABAZAKI H, HASHIMOTO T, SKELDON P. Effects of fluoride ions in the growth of barrier-type films on aluminium [J]. Electrochimica Acta, 2017, 245: 854–862.
- [22] YEROKHIN A L, SHATROV A, SAMSONOV V, SHASHKOV P, PILKINGTON A, LEYLAND A, MATTHEWS A. Oxide ceramic coatings on aluminium alloys produced by a pulsed bipolar plasma electrolytic oxidation process [J]. Surface and Coatings Technology, 2005, 199: 150–157.
- [23] HAKIMIZAD A, RAEISSI K, SANTAMARIA M, ASGHARI M. Effects of pulse current mode on plasma electrolytic oxidation of 7075 Al in Na₂WO₄ containing solution: From unipolar to soft-sparking regime [J]. Electrochimica Acta, 2018, 284: 618–629.
- [24] SIMCHEN F, SIEBER M, LAMPKE T. Electrolyte influence on ignition of plasma electrolytic oxidation processes on light metals [J]. Surface and Coatings Technology, 2017, 315: 205–213.
- [25] MARTIN J, NOMINÉ A, BROCHARD F, BRIANÇON J L, NOËL C, BELMONTE T, CZERWIEC T, HENRION G. Delay in micro-discharges appearance during PEO of Al: Evidence of a mechanism of charge accumulation at the electrolyte/oxide interface [J]. Applied Surface Science, 2017, 410: 29–41.
- [26] XIANG N, SONG R G, WANG C, MAO Q Z, GE Y J, DING J H. Formation of corrosion resistant plasma electrolytic oxidation coatings on aluminium alloy with addition of sodium tungstate species [J]. Corrosion Engineering, Science and Technology, 2016, 51: 146–154.
- [27] GEBAROWSKI W, PIETRZYK S. Influence of the cathodic pulse on the formation and morphology of oxide coatings on aluminium produced by plasma electrolytic oxidation [J]. Archives of Metallurgy and Materials, 2013, 58: 241–245.
- [28] WANG Dong-dong, LIU Xin-tong, WU Ye-kang, HAN Hui-ping, YANG Zhong, SU Yu, ZHANG Xu-zhen, WU Guo-rui, SHEN De-jiu. Evolution process of the plasma electrolytic oxidation (PEO) coating formed on aluminum in an alkaline sodium hexametaphosphate ((NaPO₃)₆) electrolyte [J]. Journal of Alloys and Compounds, 2019, 798: 129–143.
- [29] HUSSEIN R O, NIE X, NORTHWOOD D O, YEROKHIN A, MATTHEWS A. Spectroscopic study of electrolytic plasma and discharging behaviour during the plasma electrolytic oxidation (PEO) process [J]. Journal of Physics D: Applied Physics, 2010, 43: 105203.
- [30] FATKULLIN A R, PARFENOV E V, YEROKHIN A, LAZAREV M D, MATTHEWS A. Effect of positive and negative pulse voltages on surface properties and equivalent circuit of the plasma electrolytic oxidation process [J]. Surface and Coatings Technology, 2015, 284: 427–437.
- [31] BAHADOR R, HOSSEINABADI N, YAGHTIN A. Effect of power duty cycle on plasma electrolytic oxidation of A356-Nb₂O₅ metal matrix composites [J]. Journal of Materials Engineering and Performance, 2021, 30: 2586-2604.

- [32] CHENG Ying-liang, PENG Zhao-mei, WU Xiang-quan, CAO Jin-hui, SKELDON P, THOMPSON G E. A comparison of plasma electrolytic oxidation of Ti-6Al-4V and Zircaloy-2 alloys in a silicate-hexametaphosphate electrolyte [J]. Electrochimica Acta, 2015, 165: 301-313.
- [33] HASHEMZADEH M, RAEISSI K, ASHRAFIZADEH F, HAKIMIZAD A, SANTAMARIA M, LAMPKE T. Silicate and hydroxide concentration influencing the properties of composite Al₂O₃-TiO₂ PEO coatings on AA7075 alloy [J]. Coatings, 2021, 12: 33.
- [34] LI Na, YUAN Kai, SONG Ya, CAO Jin-hui, XU Jian-xiong. Plasma electrolytic oxidation of Zircaloy-2 alloy in potassium hydroxide/sodium silicate electrolytes: The effect of silicate concentration [J]. Boletín de La Sociedad Española de Cerámica y Vidrio, 2021, 60: 328–336.
- [35] USMAN B J, SCENINI F, CURIONI M. Corrosion testing of anodized aerospace alloys: comparison between immersion and salt spray testing using electrochemical impedance spectroscopy [J]. Journal of the Electrochemical Society, 2020, 167: 041505.
- [36] LEE H S, SINGH J K, ISMAIL M A. An effective and novel pore sealing agent to enhance the corrosion resistance performance of Al coating in artificial ocean water [J]. Scientific Reports, 2017, 7: 41935.
- [37] LAKSHMI R V, ARUNA S T, ANANDAN C, BERA P, SAMPATH S. EIS and XPS studies on the self-healing properties of Ce-modified silica-alumina hybrid coatings: Evidence for Ce(III) migration [J]. Surface and Coatings Technology, 2017, 309: 363–370.
- [38] ATLAS L M, NAGAO H, NAKAMURA H H. Control of dielectric constant and loss in alumina ceramics [J]. Journal of the American Ceramic Society, 1962, 45: 464–471.
- [39] DEHNAVI V, SHOESMITH D W, LUAN B L, YARI M, LIU X Y, ROHANI S. Corrosion properties of plasma electrolytic oxidation coatings on an aluminium alloy: The effect of the PEO process stage [J]. Materials Chemistry and Physics, 2015, 161: 49–58.
- [40] LIU Chen, LIU Peng, HUANG Zhi-quan, YAN Qin, GUO Ren-ge, LI Da-long, JIANG Gui-rong, SHEN De-jiu. The correlation between the coating structure and the corrosion behavior of the plasma electrolytic oxidation coating on aluminium [J]. Surface and Coatings Technology, 2016, 286: 223–230.
- [41] NOMINÉ A, NOMINÉ A V, BRAITHWAITE N S J, BELMONTE T, HENRION G. High-frequency-induced cathodic breakdown during plasma electrolytic oxidation [J]. Physical Review Applied, 2017, 8: 031001.
- [42] ROGOV A B, YEROKHIN A, MATTHEWS A. The role of cathodic current in plasma electrolytic oxidation of aluminum: Phenomenological concepts of the "soft sparking" mode [J]. Langmuir, 2017, 33: 11059–11069.
- [43] CAMA J, GANOR J. The effects of organic acids on the dissolution of silicate minerals: A case study of oxalate catalysis of kaolinite dissolution [J]. Geochimica et Cosmochimica Acta, 2006, 70: 2191–2209.
- [44] GEBAROWSKI W, PIETRZYK S. Growth characteristics of the oxide layer on aluminium in the process of plasma electrolytic oxidation [J]. Archives of Metallurgy and Materials, 2014, 59: 407–411.

- [45] JOHNSON S B, YOON T H, KOCAR B D, BROWN G E.
 Adsorption of organic matter at mineral/water interfaces.
 2: Outer-sphere adsorption of maleate and implications for dissolution processes [J]. Langmuir, 2004, 20: 4996–5006.
- [46] CHENG Ying-liang, WU Fan, DONG Jia-li, WU Xiang-quan,

XUE Zhi-gang, MATYKINA E, SKELDON P, THOMPSON G E. Comparison of plasma electrolytic oxidation of zirconium alloy in silicate and aluminate-based electrolytes and wear properties of the resulting coatings [J]. Electrochimica Acta, 2012, 85: 25–32.

阴极脉冲参数对等离子体电解氧化制备 自修复 Al₂O₃-TiO₂ 涂层的影响

Mehri HASHEMZADEH^{1,2}, Keyvan RAEISSI¹, Fakhreddin ASHRAFIZADEH¹, Frank SIMCHEN², Amin HAKIMIZAD³, Monica SANTAMARIA⁴, Thomas LAMPKE²

- 1. Department of Materials Engineering, Isfahan University of Technology, Isfahan 84156-83111, Iran;
 - Materials and Surface Engineering Group, Institute of Materials Science and Engineering, Chemnitz University of Technology, Chemnitz 09107, Germany;
- 3. Yekta Mobaddel Pars Co., Science and Technology Campus, Yazd University, Yazd 89158-18411, Iran;
- 4. Dipartimento di Ingegneria, Università di Palermo, Viale Delle Scienze, Ed. 6, 90128, Palermo, Italy

摘 要:在含草酸钛钾(Potassium titanyl oxalate, PTO)的硅酸盐电解液中采用不同阴极占空比和阴极电流密度的脉冲双极波形,在 7075 铝合金上生长等离子电解氧化(Plasma electrolytic oxidation, PEO)涂层,研究阴极脉冲参数对PEO 涂层的影响。通过扫描电子显微镜、能量色散 X 射线光谱(EDS)和 X 射线衍射(XRD)对涂层进行了表征。使用电化学阻抗谱(Electrochemical impedance spectroscopy, EIS)研究其电化学性能。结果表明,当阴极占空比和阴极电流密度分别从 20%和 6 A/dm²增加到 40%和 12 A/dm²时,内层的生长速率从 0.22 μ m/min 提高到 0.75 μ m/min。向电解液中加入 PTO 增强了阴极脉冲的影响,由此产生的阴极脉冲参数的变化使得内层生长速率从 0.25 μ m/min增加到 1.10 μ m/min。EDS 分析结果表明,Si 和 Ti 主要分布在涂层的上部。XRD 仅检测到 γ -Al₂O₃,未检测到与Ti 和 Si 化合物相关的峰。然而,EIS 结果证实,Ti⁴+掺入氧化铝改变了涂层的电性能。在含有 PTO 的电解液中使用 40%阴极占空比和大于 6 A/dm² 电流密度的双极波形获得的涂层,在 240 d 的浸泡期间表现出优异的电化学行为,这归因于有效的修复机制。关于研究参数对涂层性能的影响,强调了阴极脉冲参数和 PTO 在 PEO 过程中的作用。

关键词: Al₂O₃-TiO₂ 涂层; 等离子电解氧化; 草酸钛钾; 电化学阻抗谱

(Edited by Wei-ping CHEN)